(2)

SRI International

Final Report • December 1989

INVESTIGATION OF SCHOTTKY BARRIERS

Mark van Schilfgaarde, Research Physicist
Physical Electronics Laboratory

SRI Project 2439

Prepared for:

Directorate of Electronic and Materials Science
AFOSR/NE
Building 410
Bolling Air Force Base
Washington, D.C 20332-6448

Attn: Major Gernot Pomrenke

Contract F49620-86-K-0018

UNCLASSIFIED
SECURITY CLASSIFICATION OF THIS PAGE

REPORT DOCUMENTATION PAGE

Form Approved
OMB No. 0704-0188

1a. REPORT SECURITY CLASSIFICATION
UNCLASSIFIED

1b. RESTRICTIVE MARKINGS

2a. SECURITY CLASSIFICATION AUTHORITY

3. DISTRIBUTION / AVAILABILITY OF REPORT
Unlimited

2b. DECLASSIFICATION / DOWNGRADING SCHEDULE

4. PERFORMING ORGANIZATION REPORT NUMBER(S)
Final Report—SRI Project 2439

5. MONITORING ORGANIZATION REPORT NUMBER(S)
AFOSR-TR- 90-0204

6a. NAME OF PERFORMING ORGANIZATION
SRI International

6b. OFFICE SYMBOL (If applicable)

7a. NAME OF MONITORING ORGANIZATION
AFOSR/NE

6c. ADDRESS (City, State, and ZIP Code)
33 Ravenswood Avenue
Menlo Park, California 94025

7b. ADDRESS (City, State, and ZIP Code)
Building 410
Bolling Air Force Base
Washington, D.C. 20332-6448

8a. NAME OF FUNDING / SPONSORING ORGANIZATION
Air Force Office of Scientific Research

8b. OFFICE SYMBOL (If applicable)
AFOSR/NE

9. PROCUREMENT INSTRUMENT IDENTIFICATION NUMBER
F49620-86-K-0018

8c. ADDRESS (City, State, and ZIP Code)
Building 410, Bolling Air Force Base
Washington, D.C. 20332-6448
Attn: Major Gernot Pomrenke

10. SOURCE OF FUNDING NUMBERS

PROGRAM ELEMENT NO.	PROJECT NO.	TASK NO.	WORK UNIT ACCESSION NO.
61102F	2306	B1	

11. TITLE (Include Security Classification)
INVESTIGATION OF SCHOTTKY BARRIERS

12. PERSONAL AUTHOR(S)
Mark van Schilfgaarde

13a. TYPE OF REPORT	13b. TIME COVERED	14. DATE OF REPORT (Year, Month, Day)	15. PAGE COUNT
Final Technical	FROM 7-17-89 TO 12-31-89	1989 December	43

16. SUPPLEMENTARY NOTATION

17. COSATI CODES			18. SUBJECT TERMS (Continue on reverse if necessary and identify by block number)
FIELD	GROUP	SUB-GROUP	KEY WORDS: Hot electron transport, Schottky barriers (numerical solution to), Boltzmann equation, Transport in high fields, Band structure (JES)
20	12		

19. ABSTRACT (Continue on reverse if necessary and identify by block number)

This final report summarizes the technical progress made under the auspices of AFOSR Contract F49620-86-K-0018. Substantial progress was made in two key areas: electronic structure studies of the Schottky barrier and transport studies.

With respect to the electronic structure component, we applied ab initio electronic structure techniques to ideal metal-semiconductor interfaces. In a study of a sequence of metal-semiconductor contacts, we are able to address the problem of Schottky barrier pinning. Another study addresses the early stages of formation of Schottky barriers. With respect to the transport component, we developed some new techniques for treating high-field transport, in particular transport through a Schottky barrier. We also examined scattering from ionized dopants in the interstitial region.

20. DISTRIBUTION / AVAILABILITY OF ABSTRACT
☒ UNCLASSIFIED/UNLIMITED ☐ SAME AS RPT. ☐ DTIC USERS

21. ABSTRACT SECURITY CLASSIFICATION
UNCLASSIFIED

22a. NAME OF RESPONSIBLE INDIVIDUAL	22b. TELEPHONE (Include Area Code)	22c. OFFICE SYMBOL
Maj Gernot Pomrenke	(202) 767-4931	NE

DD Form 1473, JUN 86
(SRI on-line version)

Previous editions are obsolete

SECURITY CLASSIFICATION OF THIS PAGE
UNCLASSIFIED

CONTENTS

I. INTRODUCTION

This final report summarizes the technical progress made under the auspices of AFOSR Contract F49620-86-K-0018. We have accomplished much under the support of this project, as we show in this report. Because many of calculations reported here entail a very large amount of development time and computational effort, some of our most important results have been obtained only recently. Most of the papers that will issue out of this research are only now in preparation, and so this report presents the papers (in their current state of preparation) to be published under the sponsorship of this contract. The remainder of this report is therefore organized as follows: we outline the key accomplishments, conclusions obtained, and papers to be published; there follows in the appendices a reproduction of papers to be published, approximately in the form that they will be submitted.

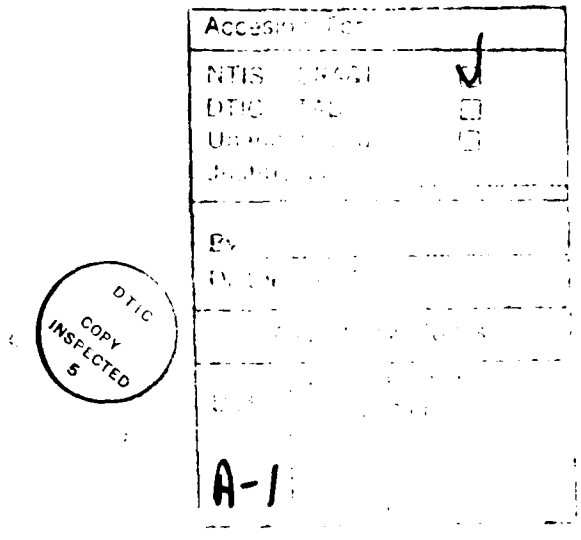

II. SUMMARY OF ACCOMPLISHMENTS

Research on this project can be grouped into two largely independent branches:

- studies related to electronic structure.
- studies related to transport.

With regard to the electronic structure, we have designed and implemented an advanced version of a band structure method known as the linear muffin tin orbitals (LMTO) method. The program we have built is quickly becoming the *de facto* standard LMTO program within the electronic structure community. This LMTO program was developed in Stuttgart in collaboration with O. K. Andersen, the originator of the LMTO and LAPW methods. It is now the standard LMTO program used by Stuttgart, and distributed by them. It is also used by several groups in the United States, including among others F. Herman at IBM Almaden (magnetic multilayers), the group of B. Segall at Case Western Reserve (studies of semiconductor alloys), and the group of D. de Fontaine at Berkeley (studies of metal alloys).

As our first application of this program, we address the highly controversial issue of the origin of pinning of the Schottky barrier in metal–semiconductor junctions. The paper reproduced in Appendix A reports the key findings of this computationally intensive study* of a number of metal/GaAs systems. We show that the metal-semiconductor interface exhibits strong pinning of the Schottky barrier, but that the "intrinsic" pinning position depends on the metal overlayer, as does the interfacial density of states (DOS). Consequences to the currently prevailing theories of the origin of Schottky barrier pinning are discussed. This paper is intended for submission to *Physical Review Letters*; another paper showing the influence of defect near the junctions was submitted to the 1990 PCSI conference.

A related study using the LMTO programs was done in collaboration with John Klepeis at Stanford University. In this study we attempted to trace the evolution of pinning the free GaAs surface as small numbers of aluminum atoms are deposited. By comparing the total energies, we found that the aluminum prefers to sit above the gallium site, rather than the arsenic, in agreement with tight-binding calculations. We have found that the interfacial dipole rapidly evolves in the 1/8 to 2 monolayer range, also in accord with tight-binding calculations. We expect to determine the defect level of aluminum on GaAs at low metal coverages, though that calculation is incomplete as of this writing, owing once again to the extremely large amount of computation for

* Approximately 1000 Cray YMP hours were consumed in the course of this calculation.

he cases of low coverage. A paper was submitted to the 1990 PCSI conference on this subject; this paper (in its current status) is reproduced in Appendix B. The completed calculations will be reported at the PCSI conference.

The last work related to the electronic structure component of this project is an outline of a technical paper on the downfolding within the LMTO method. That work was indispensible for the above interface studies, because it allowed us to reduce the number of orbitals in a (Ga,As) pair to 16 with no loss of precision. This paper (Appendix C) is intended for submission to *Phys. Rev. B.*

With respect to transport, our ultimate goal was to make realistic calculations of the electrical current-voltage characteristics in Schottky barriers. Although detailed calculation proved to be exceedingly difficult, we accomplished a great deal in pursuit of this goal. First it was necessary to solve the Boltzmann transport equations under fields that were both very large and spatially varying. Our first attempts, along traditional lines of solving the equations iteratively, proved intractable for the kinds of distribution functions emerging from a Schottky barrier. However, an alternative method to solve the Boltzmann equation was developed, in part under the auspices of this project. This method, named the "eigenvalue method," expands the distribution function in a fixed basis of functions. A normal matrix is constructed from integrals of the scattering matrix, whose eigenvector—corresponding to the zero eigenvalue—yields coefficients to the basis functions. A spatially varying distribution function is easily incorporated by allowing the basis functions to vary both in position and wave number. This method appears quite accurate and is several orders of magnitude faster than the best of other methods; in fact it is the only one so far to calculate velocity-field characteristics accurately in a semiconductor using realistic band structures and without adjustable parameters. A paper was published in *Applied Physics Letters* on this subject; another is in preparation (Appendix D) showing that this approach can be recast as a variational principle.

A second key hurdle lay in the treatment of the depletion (particularly the tunneling) region. Tunneling involves quantum processes clearly outside the domain of the Boltzmann equation. To circumvent this difficulty, we showed in the first year's report that the full problem can be divided into quasineutral and depletion regions, treating the former as a scattering problem and solving the latter with the Boltzmann equation with effective boundary conditions, determined by scattering in the depletion region.

The last difficulty arises from scattering of electrons (particularly tunneling electrons) in the depletion region. It had been argued by McGill that scattering from

the ionized dopants in the depletion region significantly alters the tunneling current in Schottky barriers, and this severely complicates studies of scattering there. We showed (last year's report; also being prepared for submission to *Applied Physics Letters*) that in fact the perturbation ionized dopants make to usually assumed quadratic potential is a small one. In a paper submitted to the 1990 PCSI (Appendix E) we estimate the scattering from a collection of ionized dopants, and show that the effect should be small.

To summarize, we believe that we overcome the principal hurdles to a reasonably precise treatment of transport through a depletion region, though a solution of the full problem, coupling quasineutral and depletion regions, has yet to be completed.

III. PRINCIPAL CONCLUSIONS

In this section we briefly summarize the principal conclusions arrived at in the course of this work. With respect to electronic structure studies:

- Schottky barriers exhibit strong pinning by the metal overlayer. Barrier heights are never determined by the "natural" band lineup, as in the classical Schottky picture.
- The "intrinsic" Fermi level tends to pin roughly at midgap in GaAs, but an exception was found in aluminum.
- The semiconductor DOS persists several layers in to the semiconductor and varies widely among the metal–GaAs systems studied.
- The last two points render implausible arguments for the universality of the pinning position being a property solely of the semiconductor band structure.
- The defect state that is ultimately responsible for pinning the Schottky barrier is the one (with sufficiently high density to shift the fermi level) farthest removed from the interface.
- Only a modest number of defects are required to pin the Schottky barrier. In light of the last two points, and also of the empirical knowledge that defects are present near the interface in certain annealing steps, it is likely that at least in some cases defects are responsible for pinning in Schottky barriers.
- The LMTO-ASA energy bands of a free GaAs (110) surface show energy bands in the forbidden gap that disappear on reconstruction, in agreement with tight-binding calculations and with experiment.
- At small coverages, LMTO-ASA calculations predict that aluminum adatoms on (110) GaAs prefer to sit over gallium sites rather than arsenic sites, in agreement with tight-binding calculations.
- The interfacial dipole is significant at 1/4 monolayer, but continues to evolve through approximately 2 ml.

With respect to studies in transport:

- The potential from a random distribution of ionized dopants deviates only slightly from the usually assumed quadratic potentials, with an average deviation less than 0.01 eV.
- There is a small correction to the average interstitial potential (and therefore the barrier height), of approximately $3/5(4\pi N_d/3)^{1/3}$. This correction is of the same order of magnitude as image-force lowering corrections, but has a weak spatial variation.
- The classical image-force lowering picture of the Schottky barrier height is incorrect. There is no dopant dependence (varying as $N_d^{1/4}$) of the image-force lowering of the Schottky barrier, because the potential maximum is determined by a combination of image-force lowering and interface states.
- Scattering from the ionized dopants in the depletion region makes a negligible correction to the classical current, and a small correction to the tunneling current.
- The problem of transport separated into a classical portion that involves the solution of the Boltzmann equation, and quantum-mechanical tunneling through the depletion region. The two couple together through effective boundary conditions to the Boltzmann equation.

- A new technique, named the "eigenvalue method," was developed to solve the Boltzmann equation. It is several orders of magnitude faster than existing approaches and has successfully been used to calculate velocity-field characteristics in semiconductors. It is readily applied to spatially varying fields, and is sufficiently fast to make tractable a detailed computation of transport through a depletion region.
- This technique can be recast as a variational principle, which ensures that the error systematically improves as basis functions are added.

IV. PAPERS SUBMITTED OR IN PREPARATION

1. M. van Schilfgaarde, "Origin of Schottky Barrier Pinning in Semiconductors," in preparation for submission to *Physical Review Letters.* (See Appendix A.)
2. M. van Schilfgaarde, "Metal-Dependence of Schottky Barrier Height in GaAs," abstract submitted to the 1990 conference *Physics and Chemistry of Semiconductor Interfaces.*
3. J. Klepeis and M. van Schilfgaarde, "Schottky Barrier Formation: Aluminum on Gallium Arsenide (110)," abstract submitted to the 1990 conference *Physics and Chemistry of Semiconductor Interfaces.* (See Appendix B.)
4. A. T. Paxton, M. van Schilfgaarde, and O. K. Andersen, "Minimal Basis Sets: Practical LMTO Downfolding," in preparation for submission to *Physical Review* **B**. (See Appendix C.)
5. M. van Schilfgaarde, "Electrostatic Potential in a Random Distribution of Ionized Dopants," in preparation for submission to the *Applied Physics Letters.* (This paper will not differ in any substantial way from last year's report.)
6. M. van Schilfgaarde, "Scattering from Ionized Dopants in Schottky Barriers," abstract submitted to the 1990 conference *Physics and Chemistry of Semiconductor Interfaces.* (See Appendix D.)
7. S. Krishnamurthy, A. Sher and A. B. Chen, "High-Field Transport in Semiconductors based on Eigenvalue Solution to Boltzmann Equation," *Appl. Phys. Lett.* **55**, 1003 (1989).
8. S. Krishnamurthy and M. van Schilfgaarde, "Variational Principle for Solution to the Boltzmann Equation," in preparation. (See Appendix E.)

Origin of Schottky Barrier Pinning in GaAs

Mark van Schilfgaarde, SRI International

333 Ravenswood Ave, Menlo Park, CA 94025

Abstract

Schottky barrier heights of five metal–GaAs interfaces are calculated self-consistently, within the local-density approximation. Pinning is strong, and all metals studied pin within the energy gap. However, the nature of interface states and the Schottky barrier height differ significantly in the systems studied. The impact these findings have on current theories of Schottky barrier formation is discussed.

Introduction

There are two major theories that purport to explain how the fermi level pins at approximately the same position in Schottky barriers. The first, due to Spicer[1], attributes the pinning to defects that form during the early stages of metal deposition. The second argues that Fermi-level pinning is an intrinsic property of the metal-semiconductor interface, and in particular depends only on the semiconductor band structure. Tejedor [2] observed that the evanescent states in the forbidden gap—tails of the metal wave functions—continually change from valence- to conduction- band character; and therefore there exists some Fermi level in the gap that makes the semiconductor locally neutral. They calculated the "neutral" point for a model metal-semiconductor junction to estimate the pinning position. As did Tejedor, Tersoff[3] conjectured that this "neutral" point was an intrinsic property of semiconductor band structure, and also argued that the neutral point could be calculated from the zero of a real-space Green's function.

Subsequently, Harrison and Tersoff [4] explicitly calculated the Schottky barrier (SB) height using a semiempirical tight-binding Hamiltonian. They found that the SB Fermi level tends to pin at the semiconductor sp^3 hybrid level E_h, rather than the "natural" Fermi level of the bulk metal E_F^0. In linear response theory, the semiconductor screens out the difference $E_F^0 - E_h$, but can do so only imperfectly because its q=0 dielectric response is finite. Thus, their calculation predicts a weak metal-dependence of the fermi level of the classical form,

$$E_F = S(E_F^0 - E_h) + E_h \tag{1}$$

with S the reciprocal of the dielectric constant, $S = 1/\epsilon$.

While their calculation is considerably more rigorous than the "neutral" point arguments, it still assumes the validity of linear response theory (this point is discussed below), and also the model is sufficiently crude that in effect there are no other parameters available to alter their conclusions.

Present Calculation

In the present work, we calculate self-consistently the metal pinning position in a series of five metals on GaAs, within the local-density approximation. We use the method of linear muffin tin orbitals (LMTO) in the atomic spheres approximation (ASA). The five metals we chose, fcc Al, Au, and Ag, and bcc Cr and Fe, all nearly lattice-match to GaAs (110) (the fcc metals lattice match by rotating them 90° about the (110) axis).

The ASA provides a convenient reference potential, to set a common scale for "natural" band lineups. Energy bands are calculated with respect to the Hartree potential on the sphere surfaces. (In a simple metal, this potential is zero.) The Fermi levels E_F^0 of bulk Al, Au, Ag, Cr and Fe were found to be –.30, –1.59, –1.17, +.63 and –.69 eV, respectively, while the valence band edge of GaAs lies at –1.32 eV. Thus $E_F^0 - E_v$ is 1.95 eV for Cr/GaAs, so a screening interfacial dipole in excess of 1 eV is necessary to pin at midgap.

Schottky barriers were calculated in a supercell geometry of n planes of metal followed by m planes of GaAs, repeating along the (110) direction. In each GaAs plane lay a (Ga,As), pair, together with two empty spheres to make bcc packing. The fcc metals contained two atoms per plane, the bcc four. The usual LMTO basis set of nine orbitals (spd) per atom was used, with the Ga, As and empty sphere d orbitals folded down (removed from the basis) using a technique essentially equivalent to the Löwdin procedure [5]. Size convergence was checked by varying n and m; those reported here had n=9 and m=9 or 13 for the fcc metals, and n=8, m=10 for the bcc. Self-consistency in the transition metals Cr and Fe was achieved only with extreme difficulty. Following the usual procedure in the atomic spheres approximation, $E_F - E_v$ was calculated by adding the self-consistent interfacial dipole to the natural band offset $E_F^0 - E_v$. $E_F - E_v$ calculated in this way also agrees with its position in the local gap of the GaAs layer farthest removed from the interface, as Figs. 1 and 2 show. The interfacial dipole is calculated by solving the Poisson equation for a self-consistent plane-averaged charge density.

The self-consistently calculated $E_F - E_v$ are displayed as a function of $E_F^0 - E_v$ in Fig. 1. It is seen that four out of the five metals studied pin at approximately

the same position in the gap. The pinning position, 0.3 to 0.4 eV above E_v, is lower than the experimentally observed value, which ranges from 0.5 to 0.75 eV. Das *et al.* [6] found a similar discrepancy in the Ni_2Si-Si interface; and the error is arguably attributable to errors in the local-density approximation. (It should be noted that 0.3 eV is approximately midgap in these calculations, because the local-density approximation underestimates the gap.) Also, because these idealized interfaces may differ considerably from the true ones, direct comparison with experiment may not be warranted. These calculations are, however, well-suited to address the issue of the universality pinning of the SB height by the intrinsic nature of the metal-semiconductor interface.

Notably Al does not pin at the same positions as the others, and moreover, examination of the planar-resolved density of states (Fig. 2) shows that the DOS near the interface are qualitatively different among the several systems studied. In Ag and Cr, for example, the Fermi level pins on a localized state that appears at midgap. The surface-states in the both the semiconducting gap and the gap separating the deep As s state and the rest of the valence band also appear very different. Because the "quasineutral" point is purely a property of the these interface states (as their role in a quasineutral theory is to redistribute the local DOS so as to make the local "neutral" point at midgap), it is improbable that there is anything universal about them, *i.e.,* that they are purely a function of the semiconductor band structure.

Fig. 1 also shows that there is no simple linear relationship between $E_F^0 - E_v$ and $E_F - E_v$, as predicted by Eq. 1. However, it is possible to calculate S, merely by making an interface self-consistent, then shifting the potential on one side by a constant amount, and observing the tendency to restore to the self-consistent value. Instead of doing so, we increased the basis set by adding f orbitals and recalculating the self-consistent Au-GaAs barrier height. This largely preserves the shape of both the Au and GaAs bands, but depresses the Au and GaAs fermi levels by 0.48 eV and 0.11 eV, respectively, for a net change in the "natural" band lineup of -0.37 eV. The recalculated pinning position changed by approximately +0.02 eV, demonstrating that the effective S for this system is large. This was checked in another way by stretching the spacing between Au layers. Stretching the spacing between layers 5% depressed the Au fermi level by 1 eV, and shifted E_F ***upward*** by 0.04 eV.

We next address the question as to what controls Fermi-level pinning when

both defect states and the "intrinsic" interface states are present. A simple model of a two-defect system, shown in Fig. 3, models the "intrinsic" interface states as a localized defect of infinite density, pinning the Fermi energy at E_F. As another plane of defects is introduced, a distance l farther away from the interface, the Fermi level shifts to E_F^*. Modeling the new defects by constant density of states n and a "charge neutrality" point E_D, E_F^* is easily found to be (in atomic Rydberg units)

$$E_F^* = \frac{E_F + (8\pi nl/\epsilon)E_D}{1 + (8\pi nl/\epsilon)}. \tag{2}$$

Provided nl is sufficiently large, the defect state will control the Fermi–level pinning, as Spicer *et. al.* [1] proposed. Actually, because of the "intrinsic" dipole shifts the Fermi–level roughly to midgap, there need not be so many defect states to pin. A defect density σl of approximately 0.01 states/ Å is sufficient to shift the fermi level 0.14 eV; assuming a modest spacing l of 10 Å, a defect density of $10^{13}/\text{cm}^2$ required. Under some annealing steps in GaAs, such a number is easily obtained.

It is clear that those innermost defect states still numerous enough to pin the fermi level ultimately control the barrier height, whether "intrinsic" or otherwise. However, because the "intrinsic" states well removed from the interface differ so widely among the various metals studied, the "quasineutral" arguments seem quite implausible.

Finally, we address why our results differ from the tight-binding analysis of Harrison and Tersoff. Since the effective interfacial dielectric constant is also large, of order 50 to 200 (depending on the metal), the large screening dipole casts doubt on the validity of linear response theory. This can be seen as follows. To apply linear response theory, one begins with a starting potential constructed, for example, by "joining and pasting" the separate bulk charge densities. This input potential is known to misalign the Fermi levels by of order 1 eV. The system responds by "screening" the Fermi level mismatch. If q=0 component of the dielectric response is of order 50, the metal-semiconductor system effectively overscreens the 1 eV mismatch by a factor of order 50. Such a perturbation is too large to be reasonably treated in linear response theory. Moreover, the simple hamiltonian in Harrison's calculation has in effect a single metal band structure (apart from a constant shift in E_F^0), so that the interfacial states all appear the same.

Conclusions

We have shown that the "intrinsic" metal-semiconductor interface exhibits strong pinning of the Fermi level, in agreement with model calculations. However, the Schottky barrier heights and the DOS near the interface differ widely among the metals studied. Thus, we conclude that the "intrinsic" states may sometimes be responsible for Fermi-level pinning, but that surface chemistry and defects are likely to play a significant role.

Acknowledgements

This work was supported by AFOSR Contract F49620-86-K-0018.

Figure Captions

Fig. 1. Self-consistently calculated Schottky barrier heights $E_F - E_v$ for five metal/GaAs junctions, in eV, plotted against the unscreened barrier height $E_F^0 - E_v$, as discussed in the text.

Fig. 2. Densities of states for selected interfaces, in arbitrary units. Fig *2a*: DOS for Au/GaAs; Fig *2b*: DOS for Al/GaAs, Fig *2c*: DOS for Cr/GaAs. Note the defect state at midgap in the Cr/GaAs junction.

Fig. 3. Simple model of "intrinsic" states coexisting with a band of defect states, as described in the text. The "intrinsic" states pin the Fermi level at E_F in the absence of defect states, but the defect states shift E_F to E_F^*.

References

1. W. E. Spicer, I. Lindau, P. R. Skeath, C. Y. Su and P. W. Chye, *Phys. Rev. Lett.* **44**, 420 (1980); W. E. Spicer, P. W. Chye, P. R. Skeath, C. Y. Su and I. Lindau, *J. Vac. Sci. Technol.* **16**, 1427 (1979).
2. C. Tejedor, F. Flores and E. Louis, *J. Phys. C* **10**, 2163 (1977).
3. J. Tersoff, *Phys. Rev. Lett.* **52**, 465 (1984).
4. W. A. Harrison and J. Tersoff, *J. Vac. Sci. Technol.* **B4**, 1068 (1986).
5. O. K. Andersen, O. Jepsen and D. Glötzel, in F. Bassani *et al.*, editors, *Highlights of Condensed Matter Theory*, Amsterdam, 1985. North Holland.
6. G. P. Das, P. Blöchl and O. K. Andersen, submitted to *Phys. Rev. Lett.*

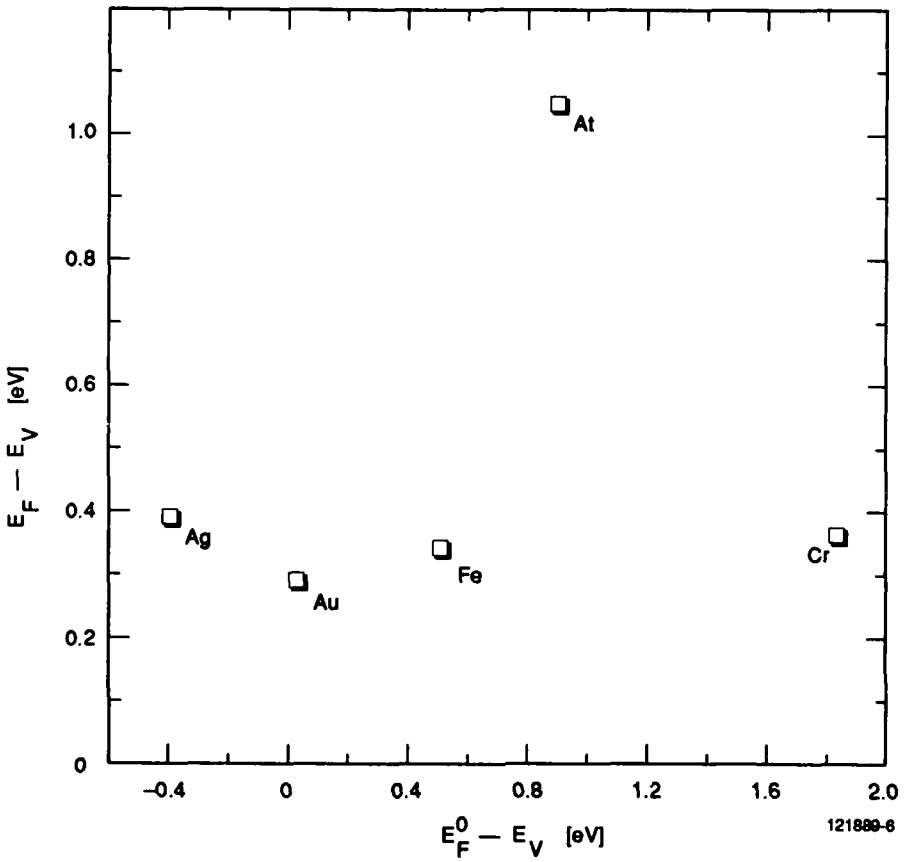
1.0
0.8
0.6
0.4
0.2
0
$E_F - E_V$ [eV]
At
Ag
Au
Fe
Cr
-0.4
0
0.4
0.8
1.2
1.6
2.0
$E_F^0 - E_V$ [eV]
121889-6

FIGURE 1

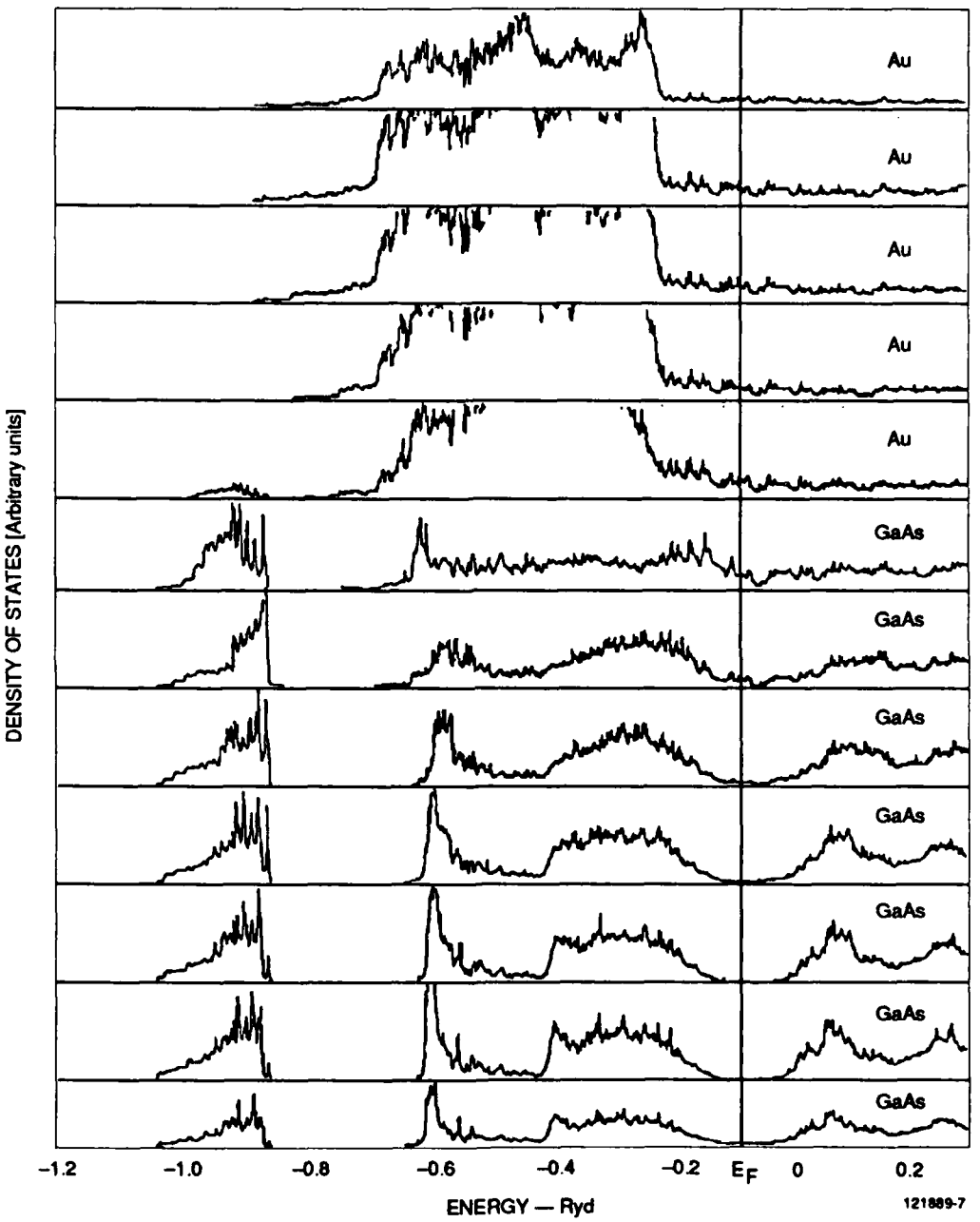

FIGURE 2
(a) Au/GaAs

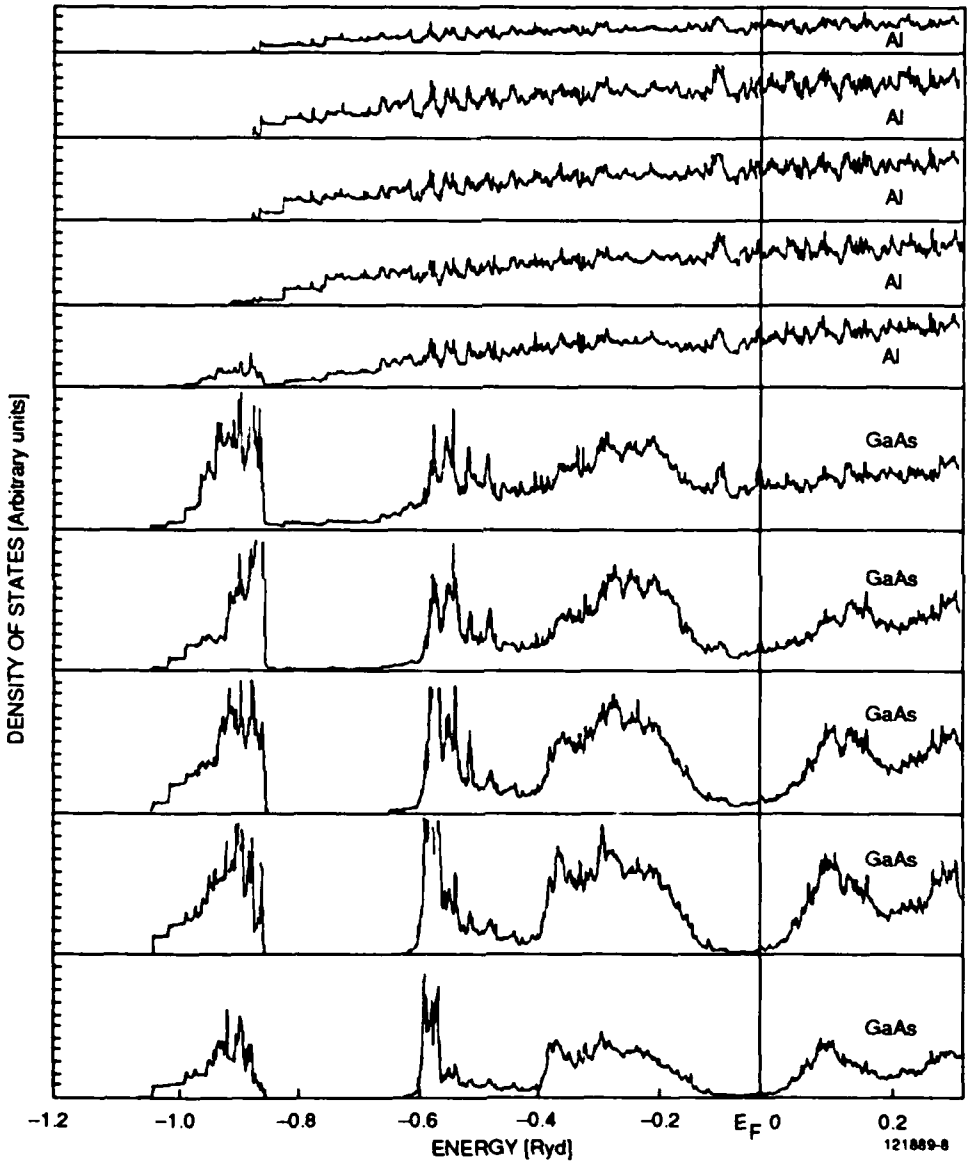

FIGURE 2
(b) Al/GaAs

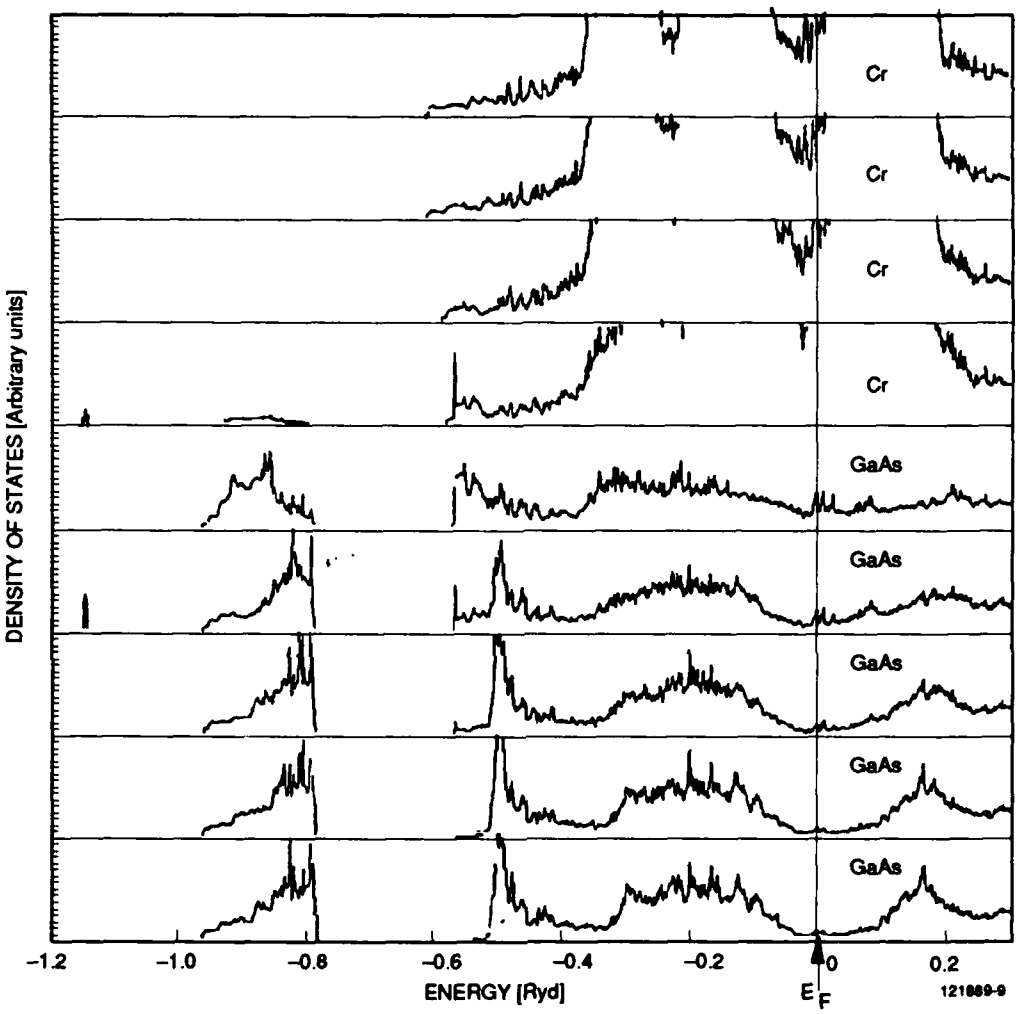

FIGURE 2
(c) Cr/GaAs

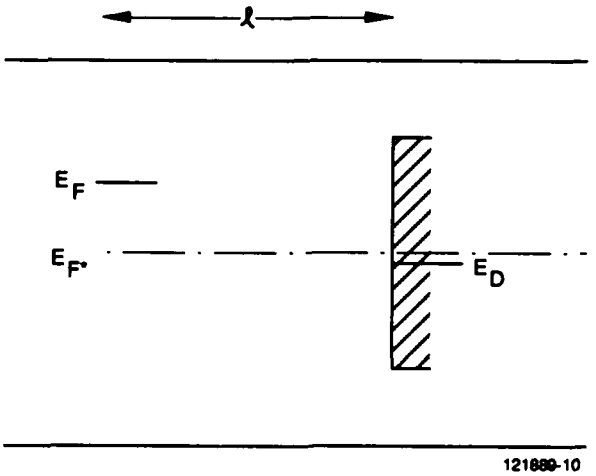

FIGURE 3

Coverage Dependence of Schottky Barrier Formation

John E. Klepeis, Lawrence Livermore National Laboratory. L-412,

P.O. Box 808, Livermore, California 94550

Mark van Schilfgaarde, SRI International

333 Ravenswood Ave, Menlo Park, CA 94025

Abstract

Self-consistent calculations of the early stages of Schottky barrier formation of Al on GaAs(110) are reported. The calculations, done within the local-density and atomic spheres approximations, confirm the tight-binding picture that potential of the first layer of GaAs deepens as Al is deposited. We also predict the Al atom favors the Ga site over the As site. We are hopeful that this approach will quantitatively predict donor and acceptor levels, and pinpoint the evolution of the interfacial dipole and the onset of metallization.

Introduction

In recent years a great deal of attention has been focused on the initial stages of Schottky barrier formation[1-8]. A number of photoemission experiments performed at liquid nitrogen temperatures on GaAs substrates and with very low metal coverages have revealed complex band-bending behavior[7,8]. The form of the band-bending curves as a function of coverage depends critically on the nature of the adatom as well as the doping of the semiconductor substrate. It is generally accepted that the observed behavior results from to the presence of either a donor or acceptor level (but not both) in the energy gap of the semiconductor bands at the surface. A detailed theory of this behavior based on simple tight-binding calculations has been presented recently[1]. The purpose of the work described in this report is to confirm and quantify the qualitative predictions of this theory using the more accurate local-density-approximation (LDA). In addition, the eventual goal is to calculate the detailed electronic structure predicted by the theory and compare the results directly with experiment. The approximate nature of a tight-binding treatment prevents such a direct comparison.

We first give a brief summary of the theory as it was presented previously[1]. It is assumed in all cases that the interaction between the adatom and the sub-

strate is nonreactive and nondestructive, so that the substrate is relatively unchanged (although small reconstructions and relaxations are not excluded). At ultra-low coverages ($\theta \leq 0.01$ ML for a doping of 10^{19} cm^{-3}) when the adatoms are isolated (*e.g.*, at low deposition temperature), there is a difference in the energy to remove an electron from the surface (donor level) and the energy to add an electron to the surface (acceptor level). Owing to the electron-electron repulsion (which is modified by the presence of the dielectric surface), the donor and acceptor levels are separated by an energy U^* which is estimated to be on the order of 1 eV. For most metals (*e.g.*, aluminum), the donor level typically comes in the energy gap with the acceptor level in the conduction band. For highly electronegative adatoms, the two levels are lower in energy relative to the surface bands, with the acceptor level in the gap and the donor level in the valence band. In either case, the absence of one of these two levels in the energy gap produces an asymmetry between the band-bending for n-type versus that for p-type; this asymmetry is observed in the photoemission experiments[7-9]. In the presence of adatom-clustering (*e.g.*, room–temperature deposition), the value of U^* is reduced so that both the donor and the acceptor level are both in the gap, producing more symmetric band-bending. A comparison between the experimentally observed variation in the donor levels for different metal adatoms at low temperatures and the results of a self-consistent tight-binding calculation[1] indicates that the experimental donor levels are probably derived from the substrate, rather than the adatom itself. However, the substrate–derived level may arise as a result of the interaction with the adatom and need not be present at the clean surface.

At higher metal coverages (0.01 ML $< \theta <$ 1 ML), the uniformly distributed adatoms are mostly neutral, but form polar bonds with the substrate. For low–electronegativity metals, these bond dipoles shift the donor and acceptor levels toward the valence band as the coverage is increased. For high–electronegativity elements the sign of the bond dipole is reversed and the shifts are toward the conduction band. We emphasize that these shifts do not arise from the charged adatoms that produced the initial band-bending, but from the bond dipoles associated with neutral adatoms. Depolarization effects eventually cause the levels to saturate as a function of coverage. The dipole shifts were found to be negligible when the adatoms are clustered.

At sufficiently high coverages ($\theta \geq 1$ ML), the wave functions of adjacent metal

adatoms overlap and the discrete donor and acceptor levels broaden into bands. The donor and acceptor bands eventually overlap and the n-type and p-type substrates are then pinned at the same position in the energy gap. The coverage at which the pinning positions converge is expected to be much higher for the clustered case than for the uniformly distributed case. In a tight-binding treatment of an ideal metal-semiconductor interface, this common pinning position is the average hybrid energy of the semiconductor[10], independent of the identity of the metal.

Tight-binding theory has the advantage of mathematical as well as conceptual simplicity and is thus ideal for a preliminary investigation that aims more toward a general understanding of trends and qualitative features rather than highly accurate numerical results. However, once this preliminary work is completed, it is desirable to have accurate results that can be compared directly to experiment and thus provide a more stringent test of the theory. The latter is the eventual goal of the work described described here.

The local approximation (LDA) to the density functional theory of Hohenberg and Kohn[11] has proven to be extremely successful in calculating the electronic structure of semiconductors[12]. However, solutions to the local-density functional are computer-intensive and limited by the constraints of computer time and memory. The use of a supercell geometry is a commom method to render tractable computation of the electronic structure of a surface. This supercell geometry consists of a periodic array of surfaces, separated by a layer of vacuum that is large enough to prevent any interaction between the two surfaces on either side. In addition, the layer of substrate must be sufficiently thick that the inner region of the substrate is bulk-like and that the surfaces on either side of the substrate interact only very weakly through the bulk. For simplicity, we make these two surfaces identical.

We consider a number of different coverages of aluminum on an ideal gallium arsenide (110) substrate. Our use of the ideal substrate is an approximation, which we will wish to relax once the initial stages of the project are completed. (In a preliminary calculation, we relaxed the a free GaAs surface. We confirmed tight-binding calculations that show the dangling bond surface states shift out of the gap.) There are two logical possibilities for the adsorption geometry on the ideal gallium arsenide (110) surface. This surface consists of zig-zag chains of gallium and arsenic atoms; each atom in a chain is bonded to two atoms in the

same chain and to one atom in the layer below. If we construct four sp^3 hybrids on each of the surface atoms, then three of these hybrids are oriented towards the three nearest-neighbors and thus contribute to the bonding levels that give rise to the valence bands. The fourth hybrid is called a "dangling hybrid" because it points toward the vacuum at an angle of 54°44' with respect to the plane of the surface. The two most likely adsorption sites are for the adatom to be bonded to either the gallium or the arsenic dangling sp^3 hybrid. We will refer to these sites as the *gallium site* and the *arsenic site,* respectively. In a previous tight-binding treatment Klepeis and Harrison[13] found that the gallium site is preferred for an isolated, neutral adatom. We will confirm this finding below but for a higher metal coverage.

The self-consistent calculations described below employ the method of linear muffin-tin orbitals (LMTO) within the atomic-spheres approximation (ASA), which "deforms" the Wigner Seitz cells into spheres of equal volume, and spheridizes the input potential inside each sphere. Empty spheres were used in the interstices and vacuum to make bcc packing. Our program implements the LMTO method in the tight-representation [14], with the usual basis set of nine *spd* orbitals per atom. All *d* orbitals were folded down using a technique essentially equivalent to Löwdin downfolding.

We define one monolayer of metal to be the coverage at which a metal adatom occupies each of the gallium and arsenic sites on the (110) surface. For one-fourth of a monolayer of aluminum, we compared the total energy (within the ASA) for the case in which the aluminum adatoms occupied half of the gallium sites with the case where half of the arsenic sites were occupied. The spacing between the adatom and the substrate was taken to be that in bulk gallium arsenide; this *ad hoc* assumption was necessary because it is not possible to determine the spacing using the ASA. We found that, for neutral aluminum adatoms, the gallium site was favored; this is consistent with the earlier tight-binding treatment[13]. In addition, the total energy difference per primitive cell (each primitive cell contained one aluminum adatom) was 0.36 eV. The tight-binding energy difference was 0.30 eV[15]. The agreement between the two results may be fortuitous because of the uncertainties in the two calculations, but the result is gratifying nevertheless. In addition, the tight-binding result is for an isolated adatom, while the LMTO calculation was for one-fourth of a monolayer where the adjacent aluminum adatoms probably interact weakly. In view of this confirmation that the

gallium site is favored at least for certain coverages, we will assume that the aluminum adatoms favor this site at all coverages. Eventually a more complete calculation should be carried out in which the surface is allowed to reconstruct and the adatom is not restricted to only two sites at a fixed distance above the surface.

Once the adatom geometry has been determined (which we have done within certain approximations), the next step is to calculate the detailed electronic structure of the surface for low metal coverages (1/4 and 1/8 ML). A number of computational difficulties arose that had to be solved before this next step could be completed. We are in the process of working out these difficulties but we can still examine the qualitative features of the preliminary results and compare them with the predictions of the earlier tight-binding treatment, as summarized above.

There is a general consensus[1-8] that aluminum deposited on gallium arsenide (110) produces a donor level in the energy gap of the semiconductor bands at the surface. Experimentally, on a *p*-type substrate, this donor level is observed to move closer to the valence band as the aluminum coverage is increased[7,8]. In terms of the theory described above, this movement arises from the electrostatic fields of the bond dipoles associated with adjacent adatoms. As the coverage is increased, the density of these dipoles increases and produces the observed motion of the donor level (see Ref. [1] for an expanded discussion). These bond dipoles are present because the bond between the aluminum adatom and the substrate gallium is polar with the charge density shifted toward the empty gallium dangling hybrid. This bond-orbital picture is borne out by the more accurate LMTO calculation.

In Table I we list the plane-averaged charges (in number of electrons) for the supercell used in this calculation. These supercells consist of four (110) gallium arsenide planes and four (110) vacuum planes. Each of these planes contains two tetrahedral sites (*e.g.*, the gallium and arsenic sites) and two interstitial sites in every primitive cell. We have performed the calculations for several different coverages: zero monolayers where the four sites in the vacuum layer next to the gallium arsenide surface are empty, a half monolayer where only the gallium site is occupied, one monolayer where both the gallium and the arsenic sites are occupied, and two monolayers where all four sites adjacent to the gallium arsenide surface contain aluminum adatoms. From Table I we see that electronic charge is transferred from the aluminum layer to the gallium arsenide surface

layer just as in the bond-orbital picture. The charge transfer is not linear in the density of aluminum adatoms, because the adatoms are interacting strongly at these coverages. Finally, we note that the nonzero planar charges for the clean surface represent the dipole contribution to the work function. The fact that the planar charge for the pure vacuum layer in Table I is so large for 2 ML indicates that we need to insert an additional vacuum layer in order to obtain accurate results.

The second qualitative feature of the theory that we can check is the sign of the energy shifts induced by the bond dipoles. In Table II we list the Madelung potentials (in Rydbergs) due to the planar charges from Table I. The zero of the Madelung potential is taken to be at the inner gallium arsenide layer. The important number to look at is the potential of the vacuum/aluminum layer. As the density of aluminum atoms increases, the potential at this layer gets deeper in energy just as the theory predicts. However, the magnitude of the shifts is on the order of one Rydberg in going from 0 ML to 2 ML which is much too large. The reason for this large shift is that the potentials in Table II do not include the intra-atomic coulomb repulsion (see Ref. 1).

In summary, we have presented the results of the preliminary stages of an LDA calculation of the electronic structure for a number of different coverages of aluminum on gallium arsenide (110). Thus far, these calculations confirm our recent tight-binding theory of the early stages of Schottky barrier formation. We are optimistic that we will realize our goal of calculating in detail the electronic structure, which can then be compared directly with experiment and thus provide a more stringent test of the theory.

Acknowledgements

This work was supported by AFOSR Contract F49620-86-K-0018.

References

1. J. E. Klepeis and W. A. Harrison, J. Vac. Sci. Technol. B7, 964 (1989).
2. I. Lefebvre, M. Lannoo, and G. Allan, (preprint).
3. W. Monch, Europhys. Lett. 7, 275 (1988).
4. K. Stiles, S. F. Horng, A. Kahn, J. McKinley, D. G. Kilday, and G. Margaritondo, J. Vac. Sci. Technol. B6, 1392 (1988).
5. M. Prietsch, M. Domke, C. Laubschat, T. Mandel, C. Xue, and G. Kaindl, Z. Phys. B74, 21 (1989).
6. K. E. Miyano, R. Cao, T. Kendelewicz, I. Lindau, and W. E. Spicer, J. Vac. Sci. Technol. A7, 731 (1989).

7. K. Stiles, A. Kahn, D. G. Kilday, and G. Margaritondo, J. Vac. Sci. Technol. B5, 987 (1987).
8. R. Cao, K. Miyano, T. Kendelewicz, K. K. Chin, I. Lindau, and W. E. Spicer, J. Vac. Sci. Technol. B5, 998 (1987).
9. D. Troost, L. Koenders, L.-Y. Fan, and W. Monch, J. Vac. Sci. Technol. B5, 1119 (1987).
10. W. A. Harrison and J. Tersoff, J. Vac. Sci. Technol. B4, 1068 (1986).
11. P. Hohenberg and W. Kohn, Phys. Rev. 136, B864 (1964).
12. See for example R. O. Jones and O. Gunnarsson, Rev. Mod. Phys. 61, 689 (1989).
13. J. E. Klepeis and W. A. Harrison, Phys. Rev. B40 (1989) (in press).
14. O. K. Andersen, O. Jepsen and D. Glötzel, in F. Bassani *et el*, editors, *Highlights of Condensed Matter Theory*, Amsterdam, 1985. North Holland.
15. J. E. Klepeis, Thesis, Stanford University (1989), pg. 170.

TABLE I : Planar averaged charges (in number of electrons). The charges listed are for a primitive cell which consists of four gallium arsenide (110) planes and four (110) vacuum planes. Each of these planes contains two tetrahedral sites (e.g. the gallium and arsenic sites) and two interstitial sites (empty spheres). Only four planes are listed because the remaining four are a mirror image of these.

Layer	*0 ML*	*1/2 ML*	*1 ML*	*2 ML*
gallium arsenide	.13	.04	-.02	-.13
gallium arsenide	-.64	-.07	.20	.80
vacuum/aluminum	.51	-.25	-.67	-1.67
vacuum	.00	.28	.49	1.01

TABLE II : Madelung potentials due to the planar charges listed in Table I. The potential is defined to be zero at the inner gallium arsenide layer. The magnitude of the shift in the potential of the vacuum/aluminum layer as the coverage is increased is large because the intra-atomic coulomb repulsion is not included.

Layer	*0 ML*	*1/2 ML*	*1 ML*	*2 ML*
gallium arsenide	.00	.00	.00	.00
gallium arsenide	-.15	-.04	.02	.15
vacuum/aluminum	.45	-.00	-.18	-.62
vacuum	.45	.32	.39	.55

Minimal Basis Sets: Practical LMTO Downfolding

A. T. Paxton and Mark van Schilfgaarde, SRI International

333 Ravenswood Ave, Menlo Park, CA 94025

O. K. Andersen, Max-Planck Institut für Festkörperforschung

7000 Stuttgart-80

These notes describe the practical considerations involved in incorporating orbital downfolding into an existing LMTO program. The starting point is assumed to be a working code in the tight-binding representation, here denoted α. However, the development is equally valid for any starting representation, so that, for example, one could set $\alpha = 0$ in all that follows.

Downfolding is effected by a basis transformation to an LMTO representation we will call β, defined as

$$\beta_l = \alpha_l; \qquad \beta_i = 1/P^0(e_\nu)$$

where l, i refer to the lower and intermediate sets respectively and α are the conventional tight-binding screening constants. The i-orbitals are those which will be downfolded so that they do not contribute to the dimension of the secular problem. $1/P^0(e_\nu)$ is the inverse potential function (which may be thought of as minus the tangent of the KKR phase shift) evaluated at e_ν.

Lambrecht and Andersen have shown that orbital downfolding amounts to a linearization of $1/P^0$ about the energy V^σ for any general representation σ, including $\sigma = 0$. V^σ is the energy at which the radial solution φ^σ has logarithmic derivative equal to ℓ.

The choice of β-representation has the main advantage that $1/P^0$ is linearized about $V^\beta = e_\nu$ which leads to the smallest error in the linear method. Two other advantages are that the moments of the charge density in the l and i sets are uncoupled; and that the i-wave eigenvectors, three-center integrals and $\dot{\beta}_i$ can be expressed in a representation-independent form (these will be discussed below).

In a self-consistent LMTO-ASA procedure, the downfolded band calculation comprises the following steps: (1). Transformation of the structure constants to the β-representation. (This depends on the potential from the previous iteration.) (2). Assembling the overlap and Hamiltonian matrices. (3). Computing

eigenvalues and eigenvectors. (4). Accumulating the moments of the new charge density.

Step (1): Transforming the Structure Constants

We begin with the Bloch-transformed, tight-binding structure constants, S^α, and their energy derivatives at $\kappa^2 = 0$, $\dot{S}^\alpha$. We need not invert the whole structure constant matrix as might appear necessary from the usual expressions for the change of basis, because only the screening constants in the i-set are different from the tight-binding values. In this case, Andersen has shown (Varenna notes, p. 103) that if we partition the structure constant matrices into square l-wave and i-wave blocks (denoted by subscripts ii and ll) connected by a rectangular il block, then defining the vector $\xi_i = (\beta_i - \alpha_i)$ and $A_{il} = (\xi_i^{-1} - S^\alpha_{ii})^{-1} S^\alpha_{il}$, one has

$$S^\beta_{ll} = S^\alpha_{ll} + (S^\alpha_{il})^\dagger A_{il}$$

and

$$S^\beta_{il} = \xi_i^{-1} A_{il}.$$

Note that in the present case, ξ_i^{-1} is the vector of inverse potential functions at e_ν, of the i-waves, in the tight-binding representation.

To transform $\dot{S}^\alpha$, we need the vector $\dot{\xi}_i = (\dot{\beta}_i - \dot{\alpha}_i)$, where the choice of $\dot{\xi}_i$ is arbitrary. We choose $\dot{\xi}_i$ so as to cause three-center overlap integrals over the i-waves to vanish as will be discussed below. If $\dot{\beta}_l = \dot{\alpha}_l$, Andersen has shown that

$$\dot{S}^\beta_{ll} = \dot{S}^\alpha_{ll} + A^\dagger_{il}\dot{S}^\alpha_{il} + (\dot{S}^\alpha_{il})^\dagger A_{il} - A^\dagger_{il}(\dot{\xi}_i^{-1} - \dot{S}^\alpha_{ii})A_{il}$$

and

$$\dot{S}^\beta_{il} = -(\dot{\xi}_i^{-1} - \dot{S}^\alpha_{ii})A_{il}.$$

where $\dot{\xi}_i^{-1} = -\xi_i^{-1}\dot{\xi}_i\xi_i^{-1}$.

Step (2): Overlap and Hamiltonian Matrices

It is convenient to divide O and H into ASA and CC (combined correction) contributions. Each of these has three terms to third-order *viz.*, one- two- and three-center integrals. Here we give explicit expressions for each of the six terms in the downfolded matrices. Due to our choice of β and $\dot{\beta}$, we may express all quantities in terms of S^β and $\dot{S}^\beta$, e_ν, and the five traditional tight-binding parameters, d^α, c^α, o^α and p^α (see Varenna notes). The reason is that it turns

out that in expressions for i-wave three-center integrals, eigenvectors and $\dot{\xi}_i$, the potential parameters appear only in the combination,

$$\frac{\sqrt{\Delta}}{C-e_\nu}=\frac{\sqrt{d^\alpha}}{c^\alpha-e_\nu},$$

which is representation-independent, and is equal to the potential parameter $\Gamma^{-\frac{1}{2}}$ when in the representation β_i (that is, when $e_\nu = V^\beta$). Thus we have, for the i-waves only,

$$\frac{\sqrt{d^\alpha}}{c^\alpha-e_\nu}=\frac{1}{\sqrt{\Gamma^\beta}}.$$

Therefore we may conveniently use the tight-binding potential parameters even for the i-waves, and in what follows we supress the superscript α on these. (This is consistent with the present development being independent of the original representation.) It is convenient to define matrices,

$$S_d \equiv \sqrt{d}S^\beta\sqrt{d} \qquad \text{and} \qquad \dot{S}_d \equiv \sqrt{d}\dot{S}^\beta\sqrt{d}$$

and for the CC-terms, we write the diagonal matrices that appear in eq. 3.87 in the Kanpur notes as follows.

$$D^{(0)}=\frac{2}{2\ell-1}\left(\frac{w}{s}\right)^{2\ell-1}$$

$$D^{(1)}=\frac{(s/w)^2}{2(2\ell+1)}+\beta\frac{2}{2\ell-1}\left(\frac{w}{s}\right)^{2\ell-1}$$

$$D^{(2)}=-\frac{1}{2(2\ell+1)^2(2\ell+3)}\left(\frac{s}{w}\right)^{2\ell+3}+\beta\frac{(s/w)^2}{2\ell+1}+\beta^2\frac{2}{2\ell-1}\left(\frac{w}{s}\right)^{2\ell-1}+w^{-2}\dot{\alpha}$$

where s and w are atomic sphere radius and average Wigner-Seitz radius. Note, they are constructed with $\dot{\alpha}$ for both the l- and i-sets (this is simply for computational convenience.) These can be made once the screening constants in the i-channels have been replaced by the inverse potential functions.

The orbitals that are folded down can only provide $\dot{\varphi}$-like tails to the basis, so that in these channels there is only an Ω matrix and no Π matrix (see eq. 2.25a in Ghent notes and eq. 2.26 in Kanpur notes). Therefore once the i-waves have been folded in to the structure constants during the basis transformation, their only explicit contributions to O and H come *via* the three-center integrals $\Omega^\dagger p\Omega$ and $\Omega^\dagger e_\nu p\Omega$ and three-center CC terms. We now choose $\dot{\xi}_i$ so that these terms in O sum to zero. By setting the terms in brackets in eq. 3.90 of the Kanpur notes to zero (with $V^\beta = e_\nu$) we arrive at the condition

$$\dot{\xi}_i=-w^2D_i^{(2)}-\frac{1}{\Gamma_i^\beta},$$

in which $\dot{\xi}_i$ depends only on representation through the explicit appearance of β in $D^{(2)}$ and not through the potential parameters.

Three-center integrals over the i-set can also be cast in a representation-independent form: using eq. 3.91 of the Kanpur notes, we have for the i-wave hamiltonian entries,

$$\sqrt{d_l}(S^{\beta}_{il})^{\dagger}\left(\frac{e_\nu - V_{\rm mtz}}{\Gamma^{\beta}_i}\right)S^{\beta}_{il}\sqrt{d_l}.$$

where $V_{\rm mtz}$ is the muffin-tin zero of energy. Note that the CC term in $D^{(2)}_i$ has been cancelled by our choice of $\dot{\xi}_i$ which has elliminated all i-wave three-center terms in O and all but the ASA three-center terms in H.

The remaining contribution to O and H come from the l-waves, and have the traditional form as follows.

Overlap ASA:

One-center	$1 + 2(c - e_\nu)o + p(c - e_\nu)^2$
Two-center	$S_d(o + p(c - e_\nu)) + (o + p(c - e_\nu))S_d$
Three-center	$S_d p S_d$

Overlap CC:

One-center	$w^2 D^{(0)} d$
Two-center	$w^2(S_d D^{(1)} + D^{(1)} S_d)$
Three-center	$w^2 S_d(D^{(2)}/d)S_d - \dot{S}_d$

Hamiltonian ASA:

One-center	$c + (c - e_\nu)(2oe_\nu + (c - e_\nu)(o + pe_\nu))$
Two-center	$S_d(\frac{1}{2} + oe_\nu + (c - e_\nu)(o + pe_\nu)) + (\frac{1}{2} + oe_\nu + (c - e_\nu)(o + pe_\nu))S_d$
Three-center	$S_d(o + pe_\nu)S_d$

Hamiltonian CC:

One-center	$V_{\rm mtz} w^2 D^{(0)} d$
Two-center	$V_{\rm mtz} w^2(S_d D^{(1)} + D^{(1)} S_d)$
Three-center	$V_{\rm mtz}(w^2 S_d(D^{(2)}/d)S_d - \dot{S}_d)$

Formulating the problem in this way has the advantage that downfolding can be incorporated into a standard tight-binding LMTO program with a minimal number of changes. The only difficult part is the scatter/gather and index point-

ing needed in partitioning the S, O and H matrices and the potential parameter, screening constant and CC vectors.

Step (3): Computing Eigenvalues and Eigenvectors

Although only the ll block of the hamiltonian is diagonalized, one may obtain an expression for the zero-order eigenvectors in the i-set in terms of the eigenvectors of the l-waves. (See, for example, Varrena notes, Eq. 147.) The success of orbital downfolding is due to the effect of the basis transformation, which is to make the tails of the $\dot{\varphi}$-like i-waves mimic as closely as possible the actual φ orbitals in the i-set had they remained in the basis. The way to achieve this is to make o^β as large as possible so that, in the transformation $\dot{\varphi}_i^\beta = \dot{\varphi}_i + \varphi_i o^\beta$ the last term dominates. In fact, in the β_i-representation in which downfolding is most effective, the conventional potential parameters d and $c - e_\nu$ are zero, while o and p are infinite. (This is why we have emphasized the use of these parameters in the original α-representation.) The first-order hamiltonian, $h^\beta = c^\beta - e_\nu + \sqrt{d^\beta} S^\beta \sqrt{d^\beta}$ is therefore zero in the i-set, but $o^\beta h^\beta$ is finite and φ_i^β can be properly normaliszd if the LMTO

$$|\chi\rangle = |\varphi_l\rangle + |\dot{\varphi}_l\rangle h_{ll} + |\dot{\varphi}_i\rangle h_{il} + |\kappa\rangle$$

becomes

$$|\chi^\beta\rangle = |\varphi_l\rangle + |\dot{\varphi}_l^\beta\rangle h_{ll}^\beta + |\varphi_i^\beta\rangle \frac{-1}{\sqrt{\Gamma_i^\beta}} S_{il}^\beta \sqrt{d_l} + |\kappa^\beta\rangle,$$

where the expansion coefficients of the φ_i^β are the correct limit of $o_i^\beta h_{il}^\beta$ (see Varenna notes p. 106).

The i-wave eigevectors, z_i in terms of the eigenvectors of the ll block of the hamiltonian, z_l are, therefore,

$$z_i(\mathbf{k}) = \frac{1}{\sqrt{\Gamma_i^\beta}} S_{il}^\beta \sqrt{d_l} z_l(\mathbf{k}).$$

Note that, again, we need only use the tight-binding potential parameters even in the i-set.

Step (4): Accumulating the charge density

Having recovered eigenvectors in the i-channels one may proceed to calculate moments of the spherical ASA charge density. Explicit expressions are given in Eq. 2.66 and 2.67 in the Kanpur notes. In the β-representation we have chosen,

there is no coupling of the moments between the l- and i-channels, because matrix elements of the first order hamiltonian, h^β are zero in the i-channels. Therefore, the moments in the l and i channels may be accumulated independently. Because the i-eigenvectors are only correct to zeroth order, their first and second moments are, in fact, not defined in any representation. However, to estimate new logarithmic derivatives (or e_ν's) for the next iteration, the first and second moments are accumulated at each k-point from the eigenvalues of the hamiltonian. Thus the moments in the i-channels are

$$m_i^0 = \sum_{n,\mathbf{k}(\text{occ.})} |z_i(\mathbf{k})|^2$$

$$m_i^r = \sum_{n,\mathbf{k}(\text{occ.})} m_i^0 (e_{n,\mathbf{k}} - e_\nu)^r \quad , \qquad r = 1, 2.$$

In this way, charge is properly distributed into the i-waves and the e_ν correctly shifted to the centers of the occupied bands during the self-consistency procedure.

Scattering from Ionized Dopants in Schottky Barriers

Mark van Schilfgaarde, SRI International

333 Ravenswood Ave, Menlo Park, CA 94025

Abstract

Using a model impurity potential from previous work [1], we estimate the scattering tunneling electrons suffer ionized dopants in the depletion region.

Introduction

A few years ago, McGill [2] calculated the scattering tunneling electrons suffer from ionized dopants in the depletion region, and determined that the effect was a large one. More recently, we showed that more careful treatment of the potential from a random distribution of ionized dopants looks very similar to a simple quadratic barrier that is usually assumed anyway. Average deviations from a quadratic potential were shown to be on the order of 0.01 eV, both by a detailed Ewald calculation with 100 randomly distributed dopants, and also with a simple model potential. On that ground, it was argued that such a perturbation would scatter only weakly. In the present work, we use the model potential as a perturbation and calculate the scattering from it.

Model Potential

In Ref. 1, an approximate perturbation to the true potential was obtained by coopting the idea of muffin-tin potentials in electronic structure calculations. Consider a single sphere of radius r_s and volume $1/N_d$, where N_d is the dopant density. The charge density inside the sphere is made out of a point charge at the center, compensated by uniform background of density N_d. The potential from all dopants is approximated as superposition of these sphere potentials. This approximation should be an excellent one for an ordered array of dopants, and is quite sufficient for our purposes. The potential for a single sphere is, in atomic Rydberg units

$$\phi(r) = \frac{2}{\epsilon r} + \frac{r^2 - 3r_s^2}{\epsilon r_s^3} - \frac{3}{5\epsilon r_s} \tag{1}$$

for $r < r_s$ and zero otherwise. Here ϵ is the dielectric constant. The last (constant) term was added to make the average perturbation zero, because the average perturbation can be added into quadratic barrier and has no effect on scattering.

Scattering Correction

Our full scattering potential is then the usual quadratic Schottky barrier, plus the small correction Eq. 1. Such a potential is well suited for the distorted wave Born approximation [3]. In that approximation, one begins with an *exact* expression for the scattering between states α and β in the presence of two potentials V_1 and V_2:

$$\langle\beta|V_1 + V_2|\alpha\rangle = \langle\beta|V_1|\alpha\rangle + \int \chi^*_{1\bar{\beta}} V_2 \chi_\alpha d\vec{r} \qquad (2).$$

The first term is the exact scattering matrix element from V_1 alone; the second is a matrix element of V_2 between the (inward travelling) scattered wave $\chi_{1\bar{\beta}}$ when scattered from V_1 alone and exact wave function χ_α, scattered by both V_1 and V_2. The Born approximation consists in this case of approximating χ_α with the wave function $\chi_{1\alpha}$ scattered by V_1 alone. For our purposes, the approximation should be an excellent one since V_2 is small.

Because the scattering rate is in proportion to $|\langle\beta|V_1 + V_2|\alpha\rangle|^2$, perturbation V_2 makes a relative change in the scattering rate of $|T_2|^2/|T_1 + T_2|^2$, where T_1 and T_2 are the first and second terms on the of Eq. 2, respectively. Let us estimate the scattering in two limits, (1) a tunneling electron very near the top of the barrier, and (2) an electron tunneling well below the barrier (electrons well above the barrier are infrequent and also their scattering is weak; they need not be considered). In either case, the rate T_1 from a true quadratic barrier is cannot be calculated analytically; however analytic solutions can be obtained when V_1 is a square well barrier, and we will consider that for the present. In the first limit, the wave functions have kinetic energy near zero, and the wave functions change slowly over the range of the impurity potential. In the limit that the wave functions χ_1 are constant, T_2 is zero (because the average of V_2 is zero, and there is no contribution from V_2). Now consider the second limit, where the wave functions are const $\times e^{-\mu z}$, with μ^2 the energy to the top of the barrier. Supposing that the square well barrier is of length L, it is straightforward to show that

$$\frac{T_1}{T_2} = \frac{9}{10\epsilon(\mu r_s)^2} e^{\mu(r_s - L)} \qquad (3)$$

For 10^{18} electrons/cm^3, r_s is about 120 au, or 60 Å— considerably less than L; thus it is clear that in this limit T_1/T_2 is exponentially small.

These limits show that impurities in the center of the depletion region scatter very little. There it is legitimate to treat the quadratic potential locally as a

square well, at least to estimate the order of magnitude of the effect. There may be some effect, however, in fluctuations of the potential near the classical turning point, *i.e.*, where the electron begins to tunnel within the barrier. To test this, we numerically solved the one-dimensional Schrödinger equation for a parabolic potential to obtain the transmission probability $|T|^2$, and then recalculated the transmission in the presence of a sine-wave perturbation. The results are shown in Fig. 1. It is seen that the curves have generally the same shape, except that the latter curve is more shallow and there is a small dip in the center, which merely reflects an effective narrowing of the barrier in those energy regions. While the effect is larger than the square-well arguments indicates, the effect here is still not all that large, since it would manifest itself as a small change in the ideality factor electrical current measurements. Moreoever, the model perturbation shown here were chosen to exaggerate the effect; the true perturbation is much smaller than this, as can be seen by examination of the the barrier in a realistic Schottky barrier.

There is, however, a correction of probably greater significance, which has to do with the classical picture of image-force lowering in Schottky barriers. In the customary picture, the quadratic barrier (whose shape derives from the ionized dopants in the depletion region) is modified because of the image potential near the interface. The metal behaves as a mirror and the electron sees as it were, a mirror image of itself, which lowers the barrier. These two potentials combine to create a maximum in the potential a few Ångstrom from the interface; this maximum can be shown [4] to vary as $N_d^{1/4}$. However, recent electronic structure calculations [5] have shown in detail how the electrostatic potential varies near the interface. The essential point is that this variation is much stronger in the few Ångstrom near the interface than the slowly varying quadratic-like potential from the ionized dopants, and therefore the shape of the potential near the maximum is governed by the interplay between the image-force potential and the electronic structure of the interface. Thus, while the image-force lowering effect is a real one, it should have no dependence on doping.

Conclusions

Scattering electrons suffer from ionized impurities in the depletion region was estimated and shown to be small, both for electrons near the top of the barrier and electrons tunneling well below the barrier. A larger effect, concerning a

correction to the classical picture of image-force lowering the Schottky barrier, was indicated.

Acknowledgements

This work was supported by AFOSR Contract F49620-86-K-0018.

Figure Caption

Fig. 1. Solid line: transmission probability of a Schottky barrier of height 1 eV, doped with 10^{18} impurities. Image-force corrections was included. Dashed line: same as above, except a perturbing sine wave potential was added. Sine wave had amplitude of 0.01 eV, period 30Å, and was placed 30Å from the interface.

References

1. M. van Schilfgaarde, in preparation for submission to *Applied Physics Letters.*
2. T. McGill, J. Vac. Sci Tech. B3, 1192 (1985)
3. L. I. Schiff, *Quantum Mechanics*, p. 327. (McGraw-Hill, New York). 1968.
4. E. H. Rhoderick, *Metal-Semiconductor Contacts*, Eq. 2.18. (Oxford University Press, Oxford). 1980.
5. M. van Schilfgaarde, abstract submitted to 1990 PCSI conference.

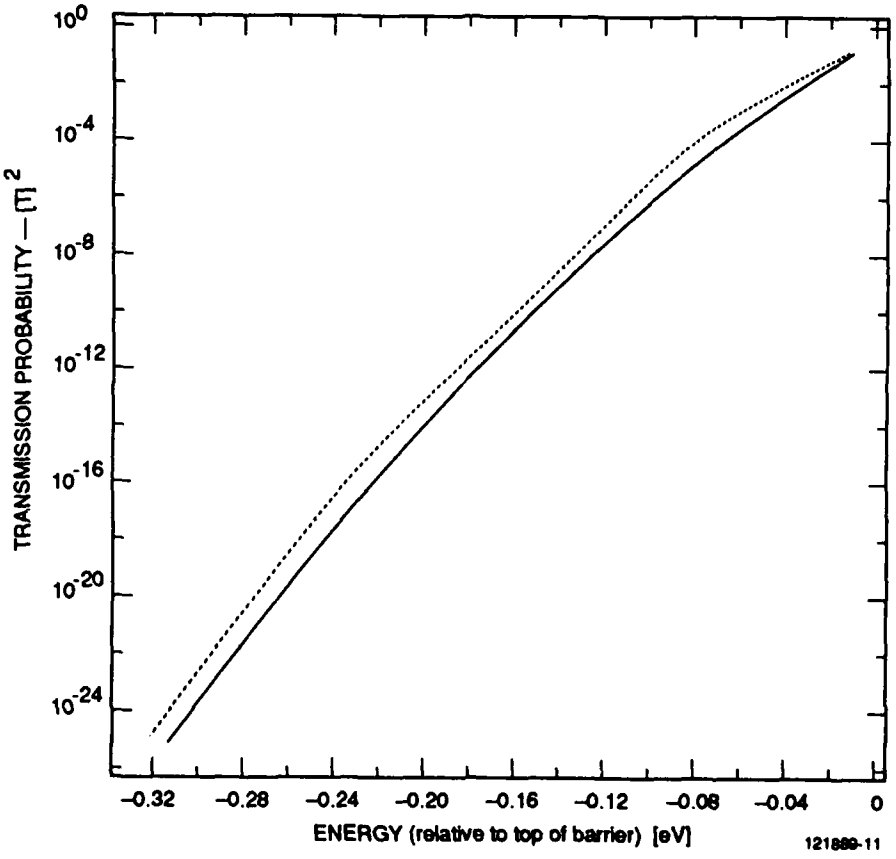
TRANSMISSION PROBABILITY — [T]^2
10^0
10^{-4}
10^{-8}
10^{-12}
10^{-16}
10^{-20}
10^{-24}
−0.32
−0.28
−0.24
−0.20
−0.16
−0.12
−0.08
−0.04
0
ENERGY (relative to top of barrier) [eV]
121889-11

FIGURE 1

Variational Principle for Solution to the Boltzmann Equation

S. Krishnamurthy and M. van Schilfgaarde, SRI International

333 Ravenswood Ave, Menlo Park, CA 94025

Abstract

We show that the basis of orthogonal Hermite polynomials can be used in the recently developed eigenvalue method [1] for solving the Boltzmann equation. A small number of basis functions is sufficient to well represent the distribution function. Calculated velocity-field characteristics agree well with experimentally measured values in GaAs. We also propose an alternative variational principle that reduces to the eigenvalue approach.

Introduction

Analytical solutions of the Boltzmann equation are limited to a few special (and unrealistic) cases. Traditionally, the most popular numerical solutions are the Monte Carlo approach [3,4] and an iterative method due to Rees [2]. Very recently, one of us [1] showed that the Boltzmann equation can be expanded in a fixed basis which leads to a highly efficient method for solving the Boltzmann equation. This approach is several orders of magnitude more efficient than other methods (*e.g.*, Monte Carlo) approach and is applicable to spatially varying fields. In the present work, we show that this new approach can be cast as a variational principle, which ensures that the solution improves as basis functions are added.

Eigenvector Approach

The steady-state Boltzmann equation is

$$\int d\vec{k}'[S(\vec{k},\vec{k}')f(\vec{k}') - S(\vec{k}',\vec{k})f(\vec{k})] = \frac{e}{\hbar}\vec{E}\cdot\nabla_{\vec{k}}f(\vec{k}). \tag{1}$$

where $f(\vec{k})$ is the distribution function and $S(\vec{k},\vec{k}')$ is the scattering rate from $\vec{k}'$ to $\vec{k}$. Let $\vec{E} = E\hat{e}_z$ and expand f in a basis set $\phi_j(\vec{k})$, *i.e.* $f(\vec{k}) = \sum_j c_j\phi_j(\vec{k})$. Then Eq. 1 reduces to

$$\sum_j \int d\vec{k}'[S(\vec{k},\vec{k}')\phi_j(\vec{k}') - S(\vec{k}',\vec{k})\phi_j(k)] - \frac{eE}{\hbar}\phi_j'(\vec{k}) = 0.$$

Operating on the above equation by $\int d\vec{k}\phi_i(\vec{k})$, we obtain

$$M_{ij}c_j = 0, \tag{2}$$

with

$$M_{ij} = \int d\vec{k} \left[\phi_i(\vec{k}) \frac{eE}{\hbar} \phi_j'(\vec{k}) - \int d\vec{k}' \left[\phi_i(\vec{k}) S(\vec{k}, \vec{k}') \phi_j(\vec{k}') - \phi_i(\vec{k}) S(\vec{k}', \vec{k}) \phi_j(\vec{k}) \right] \right]. \quad (3)$$

The solution is then the eigenvector corresponding to the zero- eigenvalue of Eq. (2). Eq. (2) was derived in Ref. 1. In practice the basis is not complete, so the Boltzmann equation is not completely satisfied. One chooses a solution with the eigenvalue nearest zero.

Numerical Results

In Ref. 1, we used the following basis functions

$$\phi_s(\vec{k}) N_s e^{-\alpha \epsilon_k} \text{ and}$$

$$\phi_p(\vec{k}) N_p \nabla \epsilon_k e^{-\beta \epsilon_k}. \quad (4a)$$

These functions yield excellent velocity-field characteristics up to about 6 kV/-cm, as Fig. 1 shows. The difficulty is that the error becomes unacceptably large for energies above 6 kV/cm. We show that similar results can be obtained using Hermite polynomials as a basis. We choose, then to expand f in the basis functions

$$\phi_j(\vec{k}) = e^{-\alpha k^2} H_{n-1}(\sqrt{2\alpha}\ \vec{k} \cdot \hat{z}). \quad (4b)$$

This choice has the advantage that we can include as many functions as we like, where the same cannot be said for the choice of Ref. 1.

Fig. 1 shows that again, the calculated drift velocity is in excellent agreement with experiment for low fields, and is in good agreement up to 6 kV/cm. But now, as the field increases, so does the number of basis functions required to get an approximately zero eigenvalue. Approximately eight functions were needed at each valley in the high-field case. (This is because these functions are not tailored to the band structure as our original choice was.) When the basis set was made too large, a zero eigenvalue was not found; this is apparently because of overcompleteness in unimportant regions of the Hilbert space of functions. To circumvent this, we propose a variational principle that should avoid numerical difficulties of the eigenvalue method, because the error should monotonically decrease as functions are added. One alternative is to employ a mixed basis, including both Equations (4a) and (4b). Another solution is to recast the problem as a variational problem, as shown below.

Variational Principle

We present a variational principle in the case the M matrix is positive definite and show that it reduces to the eigenvalue approach of Krishnamurthy *et al* in the limit that the solution is exact.

Operating on Eq. 1 by $\int d\vec{k} f(\vec{k})$ we obtain a bilinear form for the c_j

$$g \equiv \sum_{ij} c_i M_{ij} c_j = 0. \tag{5}$$

When M is positive definite *i.e.,* when it has only positive eigenvalues, Eq. (5) can never be satisfied. However one can minimize the error, which is in a root mean square sense the deviation of approximate solution from its exact one, by minimizing Eq. (5). One must impose a constraint (to avoid a trivial solution $c_j = 0$), that $\int d\vec{k} f(\vec{k})$=1. Minimization of Eq. (5) subject to this constraint, we obtain a set of simultaneous equations

$$\sum_j M_{ij} c_j = g \int d\vec{k} \phi_i(\vec{k}), \tag{6}$$

with g given as in Eq. (5). These equations reduce to the eigenvalue approach of Krishnamurthy *et al* in the limit of an exact solution ($g \rightarrow 0$).

The simultaneous equations of Eq. (6) are nonlinear. However, they can be solved by obtaining an initial guess an eigenvector from Eq. 2 (choosing the eigenvector for λ near zero), and then iteratively solving the simultaneous Eqs. (6), using the previous iteration's c_j to estimate the right-hand side.

Conclusions

We have shown that it is possible to use Hermite polynomials as an alternative basis set. While they are not so well tailored to the solution of the Boltzmann equation as are the original choice of Ref. 1 they they can be readily expanded until convergence is achieved. Some numerical difficulties with the eigenvalue approach was encountered when larger numbers of functions were used, and we present an alternative approach that uses a variational principle to guarantee convergence as basis functions are added.

Acknowledgements

This work was supported by AFOSR Contract F49620-86-K-0018.

Figure Caption

Fig 1. Calculated velocity-field characteristics as a function of applied field in GaAs.

References

1. S. Krishnamurthy, A. Sher and A. B. Chen, "High-Field Transport in Semiconductors based on Eigenvalue Solution to Boltzmann Equation," *Appl. Phys. Lett.* **55**, 1003 (1989).
2. H. D. Rees, *J. Phys. Chem. Solids* **30**, 643 (1969); H. Budd, *Phys. Rev.* **158**, 798 (1967).
3. W. Fawcett, A. D. Boardman and S. Swain, *J. Phys. Chem. Solids* **31**, 1963 (1970); W. Fawcett, D. C. Herbert, *J. Phys.* **C7**, 1641 (1974).
4. P. N. Butcher and W. Fawcett, *J. Phys. Lett.* **21**, 489 (1966).

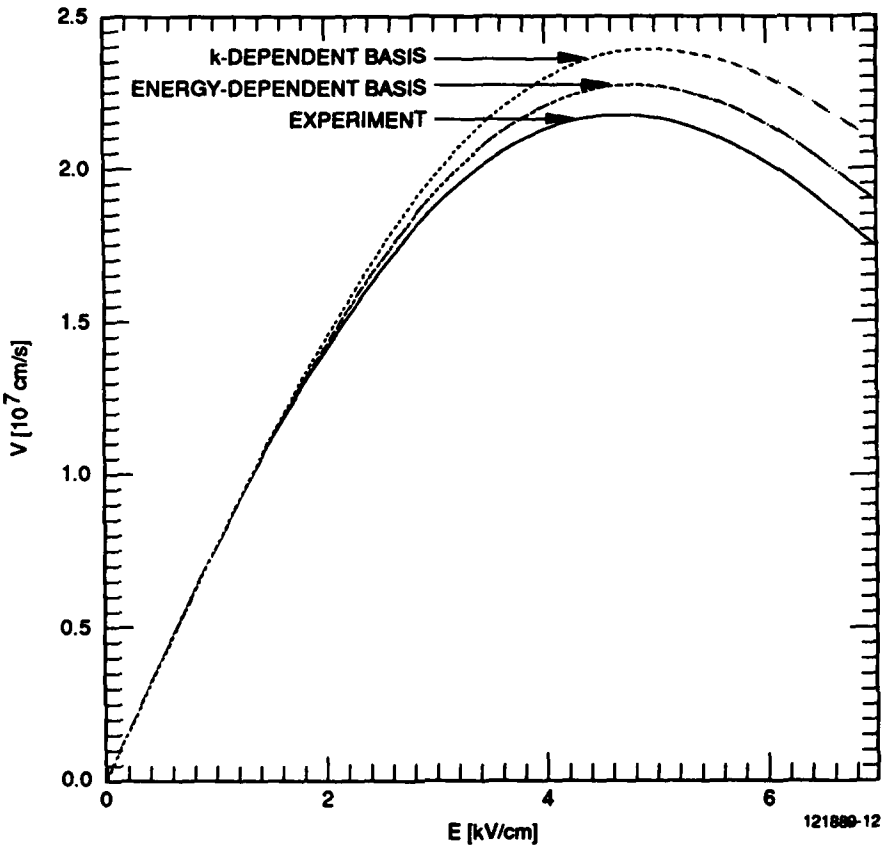
k-DEPENDENT BASIS
ENERGY-DEPENDENT BASIS
EXPERIMENT
V [10^7 cm/s]
E [kV/cm]
2.5
2.0
1.5
1.0
0.5
0.0
0
2
4
6
121889-12

FIGURE 1